Real time modulable multifocality through annular optical elements

J. Perez[1*], J. Espinosa[1], C. Illueca[1], C. Vázquez[1], and I. Moreno[2]

[1]*Departamento de Óptica, Universidad de Alicante. Carretera San Vicente del Raspeig s/n, 03690, San Vicente del Raspeig, Alicante, Spain*

[2]*Departamento de Ciencia de Materiales, Óptica y Tecnología Electrónica, Universidad Miguel Hernández, 03202, Elche, Spain*

**Corresponding author: jorge.perez@ua.es*

Abstract: We present and analyze new multifocal optical elements based on an annular distribution of the transmittance. These elements provide selectable number of foci and can be designed to work between two fixed positions or even to provide extended focal depth. The energy of the foci can be modulated through a single parameter that controls the area of each ring. In our study we analyze the quality of the peaks and also the limit number of foci that can be obtained. The properties shown by these elements make them usable in instrumental optics or in ophthalmic optics, as new intraocular implants, where multifocal elements are required. The implementation has been done on a twisted nematic spatial light modulator, thus allowing real time reconfiguration of the element.

OCIS codes: (220.3620) Lens system design; (110.2990) Image formation theory; (110.0110) Imaging systems.

References and links

1. A. Kolodziejczyk, S. Bara, Z. Jaroszewicz, and M. Sypek, "The light sword optical element -a new diffraction structure with extended depth of focus," J. Mod. Opt. **37,** 1283-1286 (1990).
2. H. Luo and C. Zhou, "Comparison of superresolution effects with annular phase and amplitude filters," Appl. Opt. **43**, 6242-6247 (2004).
3. J. Monsoriu, W. D. Furlan, P. Andrés, and J. Lancis, "Fractal conical lenses," Opt. Express **14**, 9077–9082 (2006).
4. I. Golub, "Fresnel axicon," Opt. Lett. **31**, 1890-1892 (2006).
5. V. F. Canales, and M. P. Cagigal, "Pupil filter design by using a Bessel functions basis at the image plane," Opt. Express **14**, 10393-10402 (2006).
6. T. R. M. Sales and G. M. Morris, "Diffractive superresolution elements," J. Opt. Soc. Am. A **14**, 1637-1646 (1997).
7. A. Burvall, K. Kolacz, Z. Jaroszewicz, and A. Friberg , "Simple lens axicon," Appl. Opt. **43**, 4838-4844 (2004).
8. A. Flores, M. Wang, and J. J. Yang, "Achromatic hybrid refractive-diffractive lens with extended focal length", Appl. Opt. **43**, 5618-5630 (2004).
9. J. A. Davis, C. S. Tuvey, O. López-Coronado, J. Campos, M. J. Yzuel, and C. Iemmi, "Tailoring the depth of focus for optical imaging systems using a Fourier transform approach," Opt. Lett. **32**, 844–846 (2007).
10. D. Mas, J. Espinosa, J. Perez, and C. Illueca, "Three dimensional analysis of chromatic aberration in diffractive elements with extended depth of focus," Opt. Express **15**, 17842-17854 (2007).
11. D. M. Cottrell, J. A. Davis, T. R. Hedman, and R. A. Lilly, "Multiple imaging phase-encoded optical elements written as programmable spatial light modulators," Appl. Opt. **29**, 2505–2509 (1990).
12. J. Leach, G. M. Gibson, M. Padgett, E. Exposito, G. McConell, A. J. Wright, and J. M. Girkin, "Generation of achromatic Bessel beams using a compensated spatial light modulator," Opt. Express **14**, 5581-5587 (2006).
13. C. Iemmi, J. Campos, J. C. Escalera, O. Lopez-Coronado, R. Gimeno and M. J. Yzuel, "Depth of focus increase by multiplexing programmable diffractive lenses," Opt. Express **14**, 10207-10217 (2006).
14. V. F. Canales, J. E. Oti, and M. P. Cagigal, "Three-dimensional control of the focal light intensity distribution by analytically-designed phase masks," Opt. Commun. **247**, 11-18 (2005).
15. P. J. Valle, J. E. Oti, V. F. Canales, and M. P. Cagigal, "Visual axial PSF of diffractive trifocal lenses," Opt. Express **13**, 2782–2792 (2005).
16. D. Mas, J. Pérez, C. Hernández, C. Vázquez, J. J. Miret, and C. Illueca, "Fast numerical calculation of Fresnel patterns in convergent systems," Opt. Commun. **227**, 245-258 (2003).

#92801 - $15.00 USD Received 14 Feb 2008; revised 13 Mar 2008; accepted 13 Mar 2008; published 28 Mar 2008

17. G. Mikula, Z. Jaroszewicz, A. Kolodziejczyk, K. Petelczyc, and M. Sypek, "Imaging with extended focal depth by means of lenses with radial and angular modulation," Opt. Express **15**, 9184-9193 (2007).
18. J. A. Davis, I. Moreno, and P. Tsai, "Polarization Eigenstates for Twisted-Nematic Liquid-Crystal Displays," Appl. Opt. **37**, 937-945 (1998).

1. Introduction

In the last recent years proposal of amplitude and phase only filters for designing the three dimensional response of an optical system has been a recurrent topic. Among all proposals, radial-symmetric filters have been usually preferred for the ease of its fabrication and analysis [1-5]. These filters are use in order to achieve depth of focus, achromatic system, diffractive superresolution elements, etc. [6-10]. The use of SLMs to implement diffractive optical elements (DOEs) has been reported to be a useful tool in real-time optical processing [11-13].

In some applications, e.g. in Ophthalmic Optics, a number of studies of visual performance for diffractive lenses has been developed [14]. Diffractive lenses focus light into several points simultaneously. A nearly periodic modulation of the surface of these lenses is used in order to diffract light into several directions. The two principal applications of diffractive multifocal lenses in Ophthalmology are the contact lenses and the intraocular lenses implanted during cataract surgery to replace the crystalline lens. Recently, Valle, *et al*., proposed and theoretically analyzed a diffractive trifocal lens design with adjustable add powers and light distribution in the foci [15].

The aim of this paper is to present and analyze new real time multifocal optical elements based on an annular distribution of the transmittance. In Section 2 we theoretically determine the different annular areas performance. We compute the axial intensity as well as the theoretical limit to the number of isolated foci that can be obtained. In Section 3 we give technical details of the experimental setup and results. Special attention is paid to the comparison between the experimental results and the theoretical simulations, finding a good correlation. Finally, in Section 4, we outline the main results of this paper and future works are proposed.

2. Theoretical considerations

The basic structure of the proposed elements are composed by n concentric rings with $n > 2$, each ring being characterized by its optical power P_m its boundary radial limits a_{m-1} and a_m and an amplitude function A_m. Thus, transmittance for the m-ring can be written as:

$$t_m(r) = A_m \exp\left(-j\frac{\pi}{\lambda_0}P_m r^2\right) \quad with \quad \begin{matrix} a_{m-1} \le r < a_m \\ P_n \le P_m \le P_1 \end{matrix} \quad m \in [1,n] \tag{1}$$

If we illuminate such element with a collimated monochromatic beam of wavelength λ, the obtained on-axis amplitude distribution can be written as

$$\begin{aligned} U^{ax}(z) = \frac{\pi}{j\lambda z}\sum_{m=1}^{n} A_m\left(a_m^2 - a_{m-1}^2\right)\mathrm{sinc}\left[\frac{1}{2\lambda_0}\left(\frac{\lambda_0}{z\lambda} - P_m\right)\left(a_m^2 - a_{m-1}^2\right)\right] \\ \exp\left[j\frac{\pi}{2\lambda_0}\left(\frac{\lambda_0}{z\lambda} - P_m\right)\left(a_m^2 + a_{m-1}^2\right)\right] \end{aligned} \tag{2}$$

sinc(x) being the normalized *sinc* function and λ_0 the diffractive optical element design wavelength. This expression is similar to the one obtained in [5]. From here, a convenient choice of the parameters will provide different focal structures on the optical axis. In general, such structures are used to produce focalization on a determined region of the space [13]. In our case, we pretend to cover this range of the space with a series of well-defined equidistant peaks or even with a constant focusing segment. To this end, we find that a convenient choice consists of taking a recurrence relation which, in general, takes the form:

#92801 - $15.00 USD Received 14 Feb 2008; revised 13 Mar 2008; accepted 13 Mar 2008; published 28 Mar 2008

$$P_m = P_1 - \frac{\sum_{p=1}^{m-1} g(p)}{\sum_{p=1}^{n-1} g(p)}(P_1 - P_n) \quad with \quad g(p) > 0 \tag{3}$$

with $g(m)$ being a modulation transmittance function of the m-ring. In principle, there is no restriction about the $g(p)$ function, whenever it is continuous in the [1,m-1] interval. Different $g(p)$ functions which determine the power steps between each mask zones can be used. The simplest relation is that resulting from taking $g(p)$=1, $\forall p$, which is maintained through the remaining communication.

We may consider that the shape of the whole MFM element is circular with a pupil aperture of $2R_p$. The area of each ring is directly related to the relative energy between peaks. Since the energy transmitted by the element is proportional to the area of the element, equal area ring would be the trivial solution. Nevertheless, it would be convenient to redistribute energy between the peaks. The simplest form to control the energy ratio between peaks is by redistributing the zone areas. To this end we have introduced an area modulation factor of the form:

$$\begin{aligned} S_m &= S_{m-1} + h\frac{\pi}{P_{m-1} - P_m}, \quad m \geq 2, \quad h \geq 0 \\ S_m &= \pi\left(a_m^2 - a_{m-1}^2\right), \quad S_1 = \pi a_1^2 \end{aligned} \tag{4}$$

By imposing that the outer ring is limited by the size of the element, a_n=R_p, we deduce that (see appendix):

$$a_m^2 = \frac{m}{n}R_p^2 - h\left[\frac{m}{n}\sum_{i=1}^{n-1}\frac{n-i}{P_i - P_{i+1}} - \sum_{i=1}^{m-1}\frac{m-i}{P_i - P_{i+1}}\right] \tag{5}$$

We should notice that h=0 implies that all the rings have the same area. Modifying the size of each ring will have different consequences on the energy distribution around each focus. If we consider the recurrence relation in Eq. (3), previous expression is reduced to:

$$a_m^2 = \frac{m}{n}R_p^2 - \frac{h(n-1)(n-m)m}{2(P_1 - P_n)} \tag{6}$$

The condition $a_m^2 \geq 0, \forall m$, provides an upper limit to the parameter h given by (see appendix):

$$0 \leq h \leq \frac{2(P_1 - P_n)R_p^2}{n(n-1)^2} = h_C \tag{7}$$

And, finally, by substituting Eq. (6) in Eq. (2) we obtain the axial amplitude distribution of a MFM:

$$\begin{aligned} U^{ax}(z) = &\frac{2\lambda_0\pi}{j\lambda z}\sum_{m=1}^{n} A_m \frac{1}{b_m}\operatorname{sinc}\left\{\frac{1}{b_m}\left(\frac{\lambda_0}{z\lambda} - P_m\right)\right\} \\ &\exp\left\{j\frac{\pi}{2\lambda_0}\left(\frac{\lambda_0}{z\lambda} - P_m\right)\left(\frac{(2m-1)R_p^2}{n} - h\frac{(n-1)\left[2mn + 2m - 2n - 2m^2 - 1\right]}{2(P_1 - P_n)}\right)\right\} \end{aligned} \tag{8}$$

with

#92801 - $15.00 USD Received 14 Feb 2008; revised 13 Mar 2008; accepted 13 Mar 2008; published 28 Mar 2008

$$b_m = \frac{2\lambda_0}{\left(\frac{R_p^2}{n} - h\frac{(n-1)(n-2m+1)}{2(P_1 - P_n)} \right)} \tag{9}$$

Mathematical properties of the *sinc* function state that as b_m tends to zero, the function reaches a delta peak at $z_m=\lambda_0/P_m\lambda$. Thus, for small values of b_m the axial distribution presents well defined energy peaks, each one corresponding to a different ring of the MFM. The value of b_m increases with the number of rings, being m=1 the most unfavourable case in all configurations.

In order to obtain as isolated as possible punctual peaks we must impose that side lobes of two consecutive peaks must not overlap. To this end, it is sufficient condition to impose that the first zero at right side of one peak, coincides with the first zero at left side of the following peak. As $sinc(\xi)$=0 if $\xi \in \mathbb{Z}$, the first zero on the right side of the peak number m will be taken into:

$$\frac{1}{b_m}\left(\frac{\lambda_0}{\lambda z_m^{null}} - P_m \right) = \xi \longrightarrow z_m^{null} = \frac{\lambda_0}{\lambda(P_m + b_m\xi)} \xrightarrow{\xi=-1} z_m^{null} = \frac{\lambda_0}{\lambda(P_m - b_m)} \tag{10}$$

Similarly, the first zero to the left of the peak m+1, can be found at:

$$z_{m+1}^{null} = \frac{\lambda_0}{\lambda(P_{m+1} + b_{m+1})} \tag{11}$$

Therefore, the following condition must be met:

$$z_{m+1}^{null} - z_m^{null} \geq 0 \longrightarrow P_m - b_m \geq P_{m+1} + b_{m+1} \tag{12}$$

Having (3) and (9) in mind, and after some basic mathematical manipulation, the following condition is obtained:

$$\frac{P_1 - P_n}{2\lambda_0(n-1)} \geq \frac{1}{\frac{R_p^2}{n} - h\frac{(n-1)(n-2m+1)}{2(P_1 - P_n)}} + \frac{1}{\frac{R_p^2}{n} - h\frac{(n-1)(n-2m+3)}{2(P_1 - P_n)}} \tag{13}$$

Expression (13) fulfilled for any m assuming fulfillment for m=1. That is, if it is wanted to have separate foci axis, the maximum number of foci is limited by the relation:

$$\frac{P_1 - P_n}{2\lambda_0(n-1)} \geq \frac{1}{\frac{R_p^2}{n} - h\frac{(n-1)^2}{2(P_1 - P_n)}} + \frac{1}{\frac{R_p^2}{n} - h\frac{(n^2-1)}{2(P_1 - P_n)}} \tag{14}$$

This restriction imposes a limitation on the number of zones that a MFM can admit. In Fig. 1 we depict left and right sides of the inequality (14). The limits in the number of foci for two different diameters in the particular case of h=0 are indicated there.

#92801 - $15.00 USD Received 14 Feb 2008; revised 13 Mar 2008; accepted 13 Mar 2008; published 28 Mar 2008

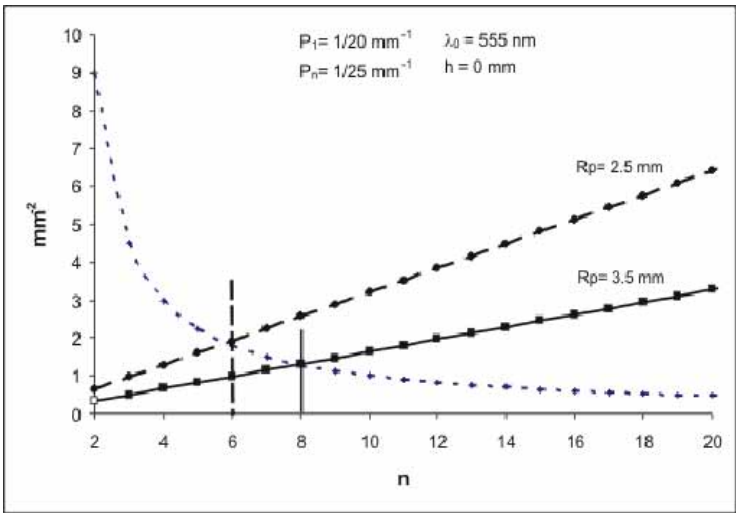

Fig. 1. Limit number of zones in a MFM according to Eq. (14). Bold lines represent the left side of the inequality for two different pupil sizes and the dot line corresponds to the right side of the inequality.

Figure 2 represents the theoretical value of the axial intensity for the case of a phase only MFM (A_m=1) with the following parameters: P_1=1/20 mm^{-1}, P_n=1/25 mm^{-1}, Rp=3.5 mm, h=0 and with a number of rings from n =2 to n=9. According to what we explained above, we can observe there that as we approach to the limit number of foci (n=8), the quality of the peaks is getting worse. For the case beyond the limit, although we obtain a series of peaks, axial aliasing does not allow multifocal implementations.

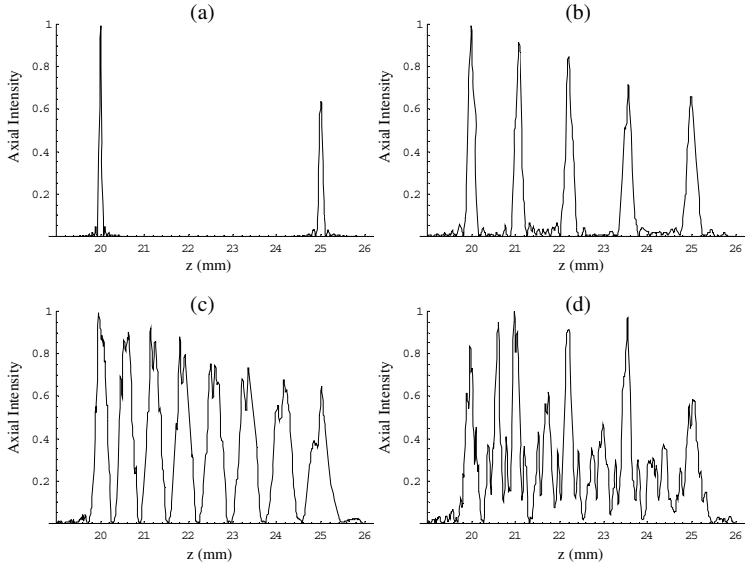

Fig. 2. Axial intensity distribution for different MFMs with the following parameters: λ=λ_0=555 nm, R_p=3.5mm, P_1=1/20 mm^{-1}, P_n=1/25 mm^{-1}, h=0 and with a number rings of n=2 (a), n=5 (b), n=8 (c) and n=9 (d).

We have also analyzed the effect of the amplitude factor A_m in the transmittance function. In Fig. 3, we compare the same phase mask with and without amplitude modulation. In Fig. 3(a), we show the axial irradiance for the only phase case. There, we can see that for the case

#92801 - $15.00 USD Received 14 Feb 2008; revised 13 Mar 2008; accepted 13 Mar 2008; published 28 Mar 2008

h=0 the intensity of the peaks diminishes for larger distances from the element. For the last peak, it is observable an amplitude decay in 40%. The equivalent case in Fig. 3(b), with a factor $A_m=1/P_m$ shows a clear stabilization of the energy of the peaks along the optical axis. Thus, this factor also acts as energy modulator. Different choices in A_m have different effects on the axial distribution energy. Nevertheless, optical implementation of amplitude and phase mask is difficult, and it results easier to implement phase only filter. That is why we have introduced the area modulation factor, as we anticipated in Eq. (4). Therefore, it is feasible to find a factor h that compensates the intensity of each focus. Taking the same parameters of the previous figures, the upper limit for h results h_C=0.00680556 mm.

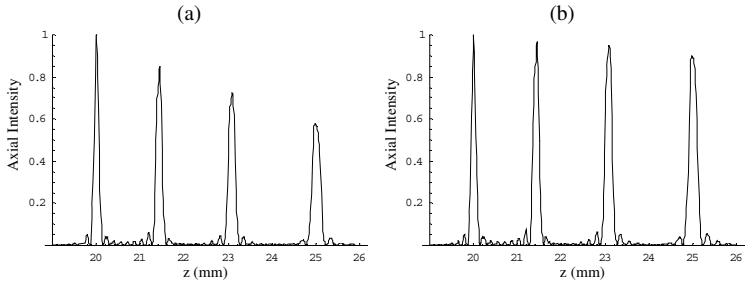

Fig. 3. Comparison between phase only MFM and hybrid amplitude and phase modulated MFM (a) A_m=1, h=0; (b) A_m=1/P_m, h=0.

With A_m=1, we have represented in Fig. 4 the axial amplitude for a 4 zones MFM for different h values. As it can be observed, changes in the value of this parameter modify the width and relative height of the peaks. One can also see that as the value of h increases, the further peaks gets higher and narrower, and the contrary happens for the closer peaks. In the limit case $h=h_C$ -see Eq. (7)- first maximum is completely lost.

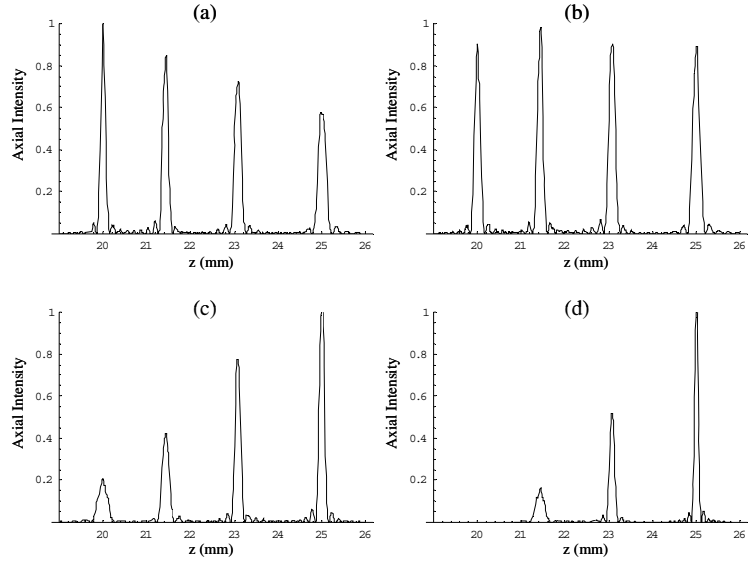

Fig. 4. Influence of modulating parameter h. (a) h=0; (b) $h=h_C/9$; (c) $h=h_C/2$; (d) $h=h_C$

Once we have defined all the parameters in the MFM determination, we have also evaluated the optical quality of the proposed element through the calculation of the MTF at each peak location. To do that, we have evaluated Fresnel patterns following the criteria

#92801 - $15.00 USD Received 14 Feb 2008; revised 13 Mar 2008; accepted 13 Mar 2008; published 28 Mar 2008

explained in [16]. In Fig. 5 we depict the radial MTF of the patterns obtained with a MFM with n=4 zones, an optical power interval of P_1=50 D, P_4=40 D, and a pupil diameter of 7.00 mm, at distances where maxima are expected (z=20.00, 21.43, 23.08 and 25.00 mm) and $h=h_C/9$.

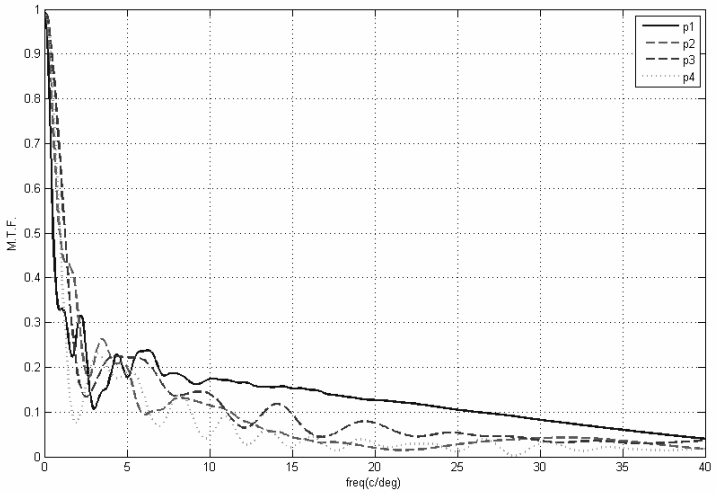

Fig. 5. Radial MTF at the focal planes (z=20.00, 21.43, 23.08 and 25.00 mm) of a MFM with n=4, *P1*=50 D, *P4*=40 D, *Rp*=3.5 mm. Legend stands for the number of peaks, being *p1* the nearest peak and *p4* the furthest one.

The presence of multiple foci degrades the MTF with respect to the one of a single lens. Fast decay in very low frequencies is due to the presence of off-axis light corresponding to defocused patterns. Thus, we expect background noise superposed to the image object. This noise can be removed by subtracting a constant value to the whole image. Comparing with other works where multifocality is proposed, we find that MFM presents slightly better response than elements presented in Iemmi, *et al*., [13] and Mikula, *et al*. [17].

It is interesting to note that, theoretically, for a large number of rings, all peaks overlap and axial distribution tends to form a continuous focal segment between two well defined distances. In Fig. 6 we present the axial intensity distribution for n=1000, $h=h_C/3$, P_1=1/20 mm^{-1} and P_n=1/25 mm^{-1}.

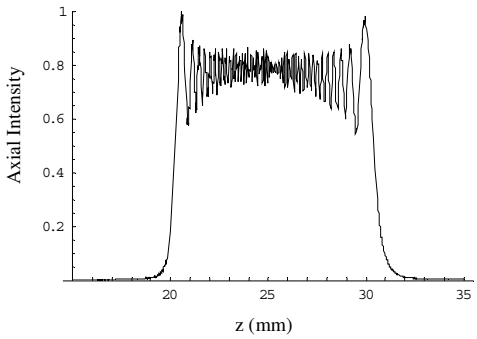

Fig. 6. Depth of focus provided by MFM with n=1000, $\lambda=\lambda_0$=555 nm, R_p=3.5mm, P_1=1/20 mm^{-1}, P_n=1/25 mm^{-1}, $h=h_C/3$.

There, one can observe that light intensity remains stable from 20 to 30 mm, which provides a focal depth of 16.7 D. Thus MFM may be used to produce very high focal depth

#92801 - $15.00 USD Received 14 Feb 2008; revised 13 Mar 2008; accepted 13 Mar 2008; published 28 Mar 2008

provided that the number of rings is high enough. This application is of major importance in ophthalmologic implants, where such elements are currently being designed.

3. Experimental results

Experimental implementation of MPMs has been done through a twisted nematic spatial light modulator (TN-SLM). Although the Nyquist limit of these modulators limits the optical power of the rings, these systems provide real time manipulation possibilities. Thus, the area of the different rings can be changed at video rate and thus increasing the applications of the MPM masks. The scheme of the experimental setup can be seen in Fig. 7. The core of the experimental setup is a twisted nematic liquid crystal display (TN-LCD) from CRL-Opto, model XGA3. This device has a resolution of 1024 x 768 squared pixels, being the pixel pitch 18x18 μm^2, the mask is addressed through a standard VGA output.

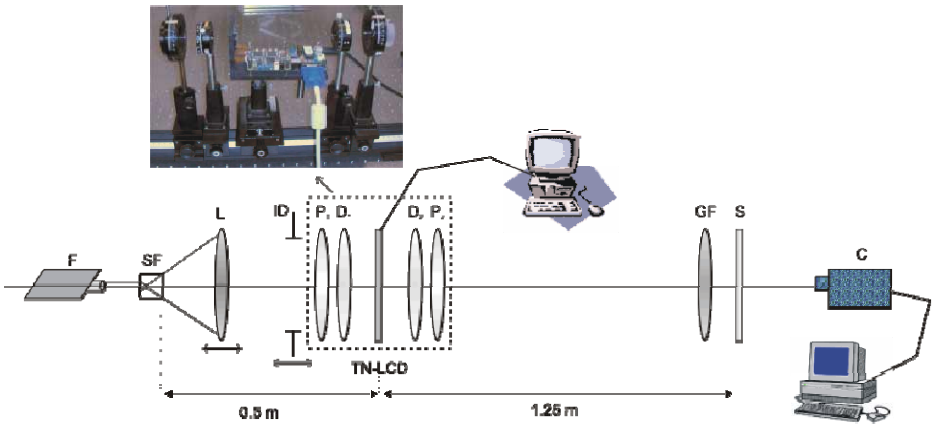

Fig. 7. Experimental apparatus for obtaining multifocal distributions: F, laser source; SF, spatial filter; L, imaging lens; ID iris diaphragm; P1, P2 linear polarizers; D1, D2, quarter wave plates; TN-LCD, twisted nematic spatial light modulator; GF gray filter; S screen; C, digital camera.

In order to use these transmission modulators as pure phase elements we used the arrangement described by J. A. Davis, *et al*., [18], who used two quarter wave-plates *D1* and *D2* and two polarizers *P1* and *P2*. Previously, the angles of these four elements were properly fitted so that the phase modulation provided by the modulator was the most efficient one for used wavelength. With the aim of achieving a relatively large phase modulation, it was used an Ar laser, *F*, of a wavelength of 488 nm together with a spatial filter, *SF*, used to expand the beam. The lens *L* with 25 cm of focal length allow to move the object point in order to obtain the images provided by the different ring on a fixed semitransparent screen *S*, located at 1.25 m from the modulator. The first polarizer was placed against an iris diaphragm, *ID*, which limits the diameter of the beam to 13.9 mm. Finally, an 8-bit camera, *C*, captured the image on *S*. In order to not saturating the image detected by the camera, a grey filter, *GF*, was located to the left of the screen.

A four zones (n=4) phase mask was implemented in the modulator. In order to conduct the experimental verification, the chosen zone powers (P_1=1.82 D, P_n=0.40 D) followed Eq. (3). Those values were limited by the number and size of the pixels of the used modulator. In Fig. 8 we represent the phase mask implemented in the modulator. The radial limits of the four areas were in this case: 2.32, 3.90, 5.43, 6.95 mm and the area parameter used for modulator was $h=h_C/1.8=0.00211425$ mm.

#92801 - $15.00 USD Received 14 Feb 2008; revised 13 Mar 2008; accepted 13 Mar 2008; published 28 Mar 2008

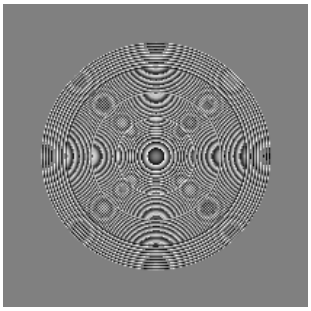

Fig. 8. Phase mask implemented in the modulator for $h=h_C/1.8$, Rp=6.95 mm, n=4, P_1=1.818 D and P_n=0.4 D.

Figure 9(a) shows the theoretical light distribution that should be collected in the four foci planes. Again, this calculation was made by using the propagation algorithm for convergent light patterns proposed by Mas, *et al*., in [16].

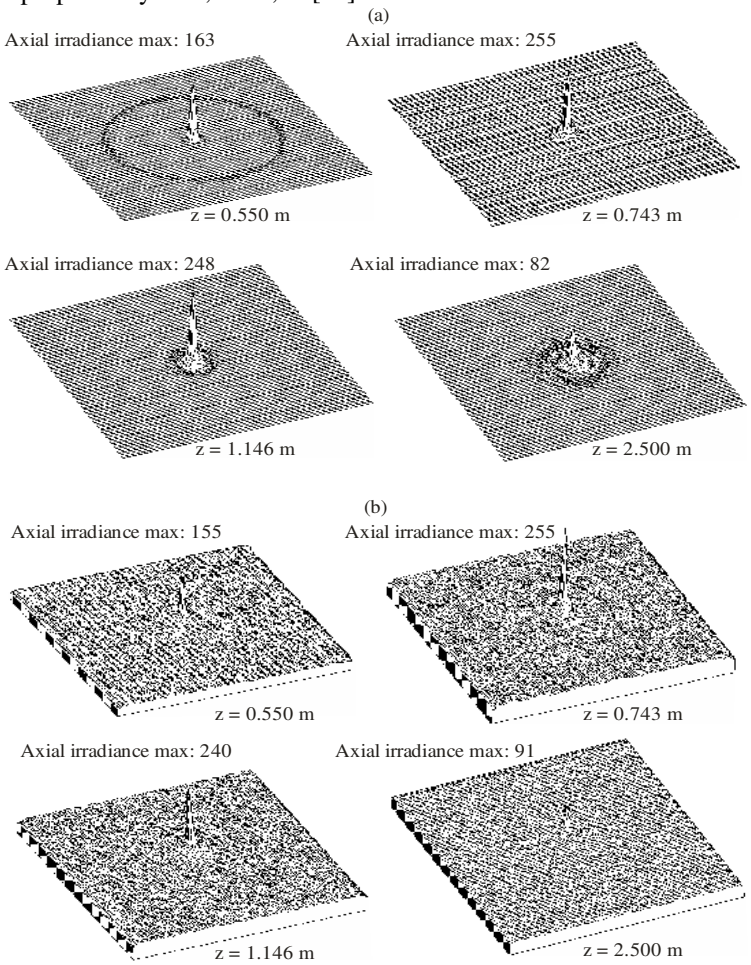

Fig. 9. (a). Calculated intensity distribution at the theoretical focus of each ring. (b). Real intensity captured with a CCD camera of a phase only MPM ($h=h_C/1.8$) implemented in a TN-LCD. Maximum values of intensity at each plane are shown.

In Fig. 9(b), we show the intensity distribution of the four foci found on the screen, S, as we varied the position of the lens L. Maximum intensity at distances, $z_i=1/P_i$ being P_i the

#92801 - $15.00 USD Received 14 Feb 2008; revised 13 Mar 2008; accepted 13 Mar 2008; published 28 Mar 2008

optical power of the *i-th* ring are shown. A simple application of Geometrical Optics laws indicates the required successive distances between the lens *L* and the spatial filter in order to obtain the different foci on the screen, depending on the powers introduced in the phase modulator. Regarding the value of the maximum peak of each focus, the theoretical calculation shows that the absolute maximum of axial irradiance for the programmed parameters corresponds to the second focus, located 734 mm from the modulator, which has been given a value of 255 (Fig. 9(a)). The grey filter *GF* has been adjusted to allow maximum response of the camera to this spot. Thus, all other registered intensities must not saturate the camera. As it can be seen in Fig. 9, the relative values between the maximum comply with the theoretical values predicted.

In order to analyze the influence of the area modulation parameter, h, we introduced a new phase distribution with the same characteristics that those previously described but with $h=h_C$ (Fig. 10).

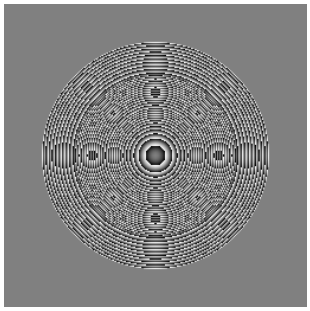

Fig. 10. Phase mask implemented in the modulator for $h=h_C$, R_p=6.95 mm, n=4, P_1=1.818 D and P_n=0.4 D.

In theory, this should lead to the elimination of the focus determined by the area with more dioptric power, corresponding to the central ring. Implementation of the new mask at the TN-LCD show that that the focus corresponding to z=0.550 m of focal length is lost. In Fig. 11(a) we can see the theoretical axial irradiance for the mask shown in Fig. 10.

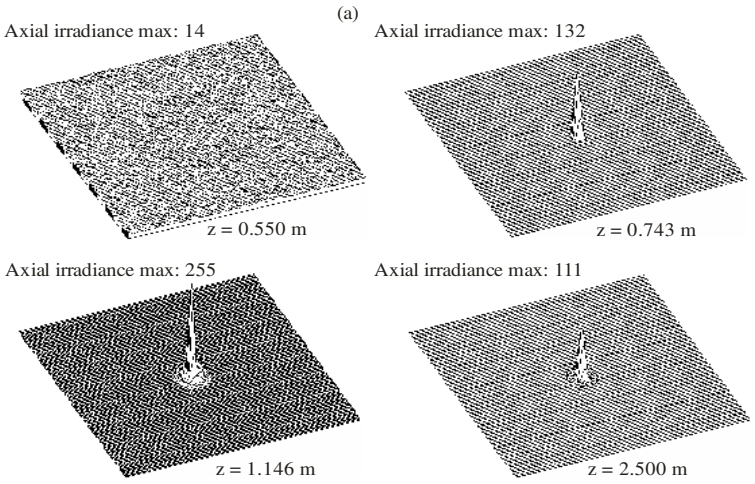

Fig. 11. (a). Calculated intensity distribution at the theoretical focus of each ring of a phase only MPM ($h=h_C$). Maximum values of intensity at each plane are shown.

#92801 - $15.00 USD Received 14 Feb 2008; revised 13 Mar 2008; accepted 13 Mar 2008; published 28 Mar 2008

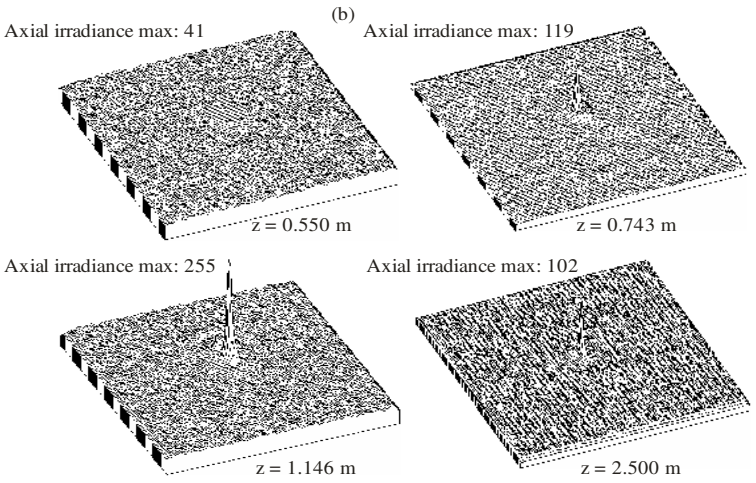

Fig. 11. (b) Real intensity captured with a CCD camera of a phase only MPM ($h=h_C$) implemented in a TN-LCD. Maximum values of intensity at each plane are shown.

The focus corresponding to a power of P_2=0.873 D (z=1.146 m) marks the absolute maximum. Figure 11(b) shows the experimental radial mean of the intensity found in the three focal planes. Note that the relative values of the maxima are consistent with those theoretically predicted.

4. Conclusions

In this work we have proposed and analyzed the optical performance of a new multifocal mask which allows modulating the relative intensity between peaks. The mask is divided in concentric rings setting the power of each zone by means of a recursive relation. We obtain a range of equidistant peaks covering a desired range with good axial resolution. Relative energy between peaks is controlled by an area modulating factor. The possibilities and limitations of the design have been also stated.

The multifocal phase mask has been experimentally implemented on a Twisted Nematic Spatial Light Modulator. This device permits changing the mask in real time, thus allowing full modulability of the element. As a future work, this real time modulable multifocal elements could be used in order to make previous studies of new multifocal lenses proposals, to analyze the depth of focus capabilities whether high zone number is used and, of course, to study the implications in imaging real scenes.

Appendix

In order to ensure clarity to the readers, in this appendix we describe the mathematical derivations realized to deduce Eq. (5) and Eq. (7).

First, in order to obtain Eq. (5), bearing in mind Eq. (4), with $m = 2$ it results:

$$\pi\left(a_2^2 - a_1^2\right) = \pi a_1^2 + h\frac{\pi}{P_1 - P_2} \longrightarrow a_2^2 = 2a_1^2 + \frac{h}{P_1 - P_2} \tag{A.1}$$

If $m = 3$ is used, it can be deduced that:

$$\begin{aligned} \pi\left(a_3^2 - a_2^2\right) = \pi\left(a_2^2 - a_1^2\right) + h\frac{\pi}{P_2 - P_3} \longrightarrow a_3^2 = 2a_2^2 + \frac{h}{P_2 - P_3} \\ a_3^2 = 3a_1^2 + h\frac{2}{P_1 - P_2} + h\frac{1}{P_2 - P_3} \end{aligned} \tag{A.2}$$

#92801 - $15.00 USD Received 14 Feb 2008; revised 13 Mar 2008; accepted 13 Mar 2008; published 28 Mar 2008

Repeating the process successively, we obtain the following recurrence relation:

$$a_m^2 = ma_1^2 + h\sum_{i=1}^{m-1}\frac{m-i}{P_i - P_{i+1}} \tag{A.3}$$

By imposing that the outer ring is limited by the size of the element, a_n=R_p, we deduce that:

$$a_n^2 = na_1^2 + h\sum_{i=1}^{n-1}\frac{n-i}{P_i - P_{i+1}} = R_p^2 \longrightarrow a_1^2 = \frac{R_p^2}{n} - \frac{h}{n}\sum_{i=1}^{n-1}\frac{n-i}{P_i - P_{i+1}} \tag{A.4}$$

expression from which we can finally deduce the equation that provides the zone radius values (Eq. (5)):

$$a_m^2 = \frac{m}{n}R_p^2 - h\left[\frac{m}{n}\sum_{i=1}^{n-1}\frac{n-i}{P_i - P_{i+1}} - \sum_{i=1}^{m-1}\frac{m-i}{P_i - P_{i+1}}\right] \tag{A.5}$$

In second place, to obtain the Eq. (7), if we consider the recurrence relation in Eq. (3) with $g(m)$=1, $\forall m$, it results:

$$P_i = P_1 - \frac{i-1}{n-1}\left(P_1 - P_n\right) \tag{A.6}$$

Therefore,

$$P_i - P_{i+1} = \left[P_1 - \frac{i-1}{n-1}\left(P_1 - P_n\right)\right] - \left[P_1 - \frac{i}{n-1}\left(P_1 - P_n\right)\right] = \frac{P_1 - P_n}{n-1} \tag{A.7}$$

Thus, expression describing the zone radius results:

$$a_m^2 = \frac{m}{n}R_p^2 - \frac{h(n-1)}{\left(P_1 - P_n\right)}\left[\frac{m}{n}\sum_{i=1}^{n-1}(n-i) - \sum_{i=1}^{m-1}(m-i)\right] \tag{A.8}$$

Making the summation, the above expression is reduced to:

$$a_m^2 = \frac{m}{n}R_p^2 - \frac{h(n-1)(n-m)m}{2\left(P_1 - P_n\right)} \tag{A.9}$$

The condition $a_m^2 \geq 0$, $\forall m$, provides an upper limit to the parameter h given by:

$$h \leq \frac{2\left(P_1 - P_n\right)R_p^2}{n(n-1)(n-m)}, \quad \forall m \tag{A.10}$$

that is the Eq. (7),

$$0 \leq h \leq \frac{2\left(P_1 - P_n\right)R_p^2}{n(n-1)(n-m)} \leq \frac{2\left(P_1 - P_n\right)R_p^2}{n(n-1)^2} = h_C \tag{A.11}$$

Acknowledgments

This work has been supported by the Ministerio de Educación y Ciencia through the projects nr. FIS2005-05053, FIS2006-13037-C02-02 and by the University of Alicante through the project GRE07-7P.

#92801 - $15.00 USD Received 14 Feb 2008; revised 13 Mar 2008; accepted 13 Mar 2008; published 28 Mar 2008